Thermal Distribution of Temperature Rise for 18V Cordless Impact Drill

by

Syed Naufal Bin Syed Ahmad Alhabshi

Dissertation submitted in partial
fulfilment of the requirements for the
Bachelor of Engineering (Hons)
(Mechanical Engineering)

SEPTEMBER 2012

Universiti Teknologi PETRONAS
Bandar Seri Iskandar
31750 Tronoh
Perak Darul Ridzuan

CERTIFICATION OF APPROVAL

Thermal Distribution of Temperature Rise for 18V Cordless Impact Drill

by

Syed Naufal Bin Syed Ahmad Alhabshi

A project dissertation submitted to the
Mechanical Engineering Programme
Universiti Teknologi PETRONAS
In partial fulfilment of the requirement for the
BACHELOR OF ENGINEERING (Hons)
(MECHANICAL ENGINEERING)

Approved by,

_____

(Dr Suhaimi Hassan)

CERTIFICATION OF ORIGINALITY

This is to certify that I am responsible for the work submitted in this project, that the original work is my own except as specified in the references and acknowledgements, and that the original work contained herein have not been undertaken or done by unspecified sources or persons.

_____

(SYED NAUFAL BIN SYED AHMAD ALHABSHI)

ABSTRACT

Cordless impact drill is used today by industry professionals to drive big screws, tighten and loosen bolts with high speed. High temperature is one of the sources failures of this tool and the development of thermal design methodologies for cordless impact drills still is not renowned. The aims of this project are to determine the temperature profile of selected components, to produce simulation work on temperature profile and to determine the most suitable method of temperature measurement of cordless drill temperature rise test. After acquiring the necessary tools and materials, metal bolting test is done using thermocouples and data logger, and then repeated using different material (Jelutong wood) and different temperature measurement method (Infrared thermo graphic camera). The test results are validated by a simulation of the thermal transient for the tool housing using ANSYS by means of Finite-Element Analysis (FEA). As the results, temperature profiles for selected components were drawn showing that metal bolting process generated more heat than that of wood bolting. The gearbox was the hottest part of the tool (130ºC), followed by the motor (116ºC). Thermocouple and data logger assembly was proven well suited for components' temperature measurement than that of thermo graphic imaging. Nevertheless the latter is accurate for surface temperature measurement and useful for simulation validation. This project successfully proposed a general approach to modeling temperature rise phenomena in cordless impact drill, and demonstrated the thermal transient across the tool housing.

ACKNOWLEDGEMENT

In the name of Allah S.W.T, the Almighty, the Most Gracious and Most Merciful, with the Selawat and Salam to Prophet Muhammad SAW.

Alhamdulillah, I express my first and forever gratitude to Allah SWT who bless me with wisdom, commitment and the strength for He who is Ever All-Powerful, All-Wise.

Second, I would like to express my utmost appreciation and sincere "Thank you" to my supervisor, Dr Suhaimi Hassan, who found time in his busy schedule to guide me, monitors my progress and answers my questions. His passion for this project progress really inspired me. I am also deeply grateful for his advice, encouragement and patience throughout the duration of the project work.

Third, my gratitude goes to Mr Mohd Faizairi Bin Mohd Nor, for he has shared his valuable advice and expertise in handling the infrared thermo graphic camera to validate my experiment.

Fourth, I would like to thank all the lecturers and supporting technicians in Mechanical Engineering department, especially to Dr. Mokhtar B Awang, and Dr. Saravanan A/L Karuppanan for their guidance and knowledge sharing.

Fifth, I am grateful to Bosch Power Tools Engineering Penang Staff, for their help and sharing their great technical knowledge in their field of expertise.

Sixth, I thank my parents, Syed Ahmad Bin Syed Idrus Alhabshi and Sharifah Nor Ashikin S.A. Rahman and all my family members for the forever love and support they have given me.

Seventh, I would like to thank my colleagues; who share their opinions and give a helping hand for the project success and for the warm friendship.

TABLE OF CONTENT

LIST OF FIGURES

LIST OF TABLES

CHAPTER 1: INTRODUCTION

1.1 Introduction

Cordless impact drill is a power tool that is commonly used today by industry professionals to drive big screws, tighten/loose bolts with high speed. By definition, a cordless impact drill is an electric impact drill which uses rechargeable 18V Lithium ion (Li-OH) battery packs. Common cordless drills found today use three-phase induction motors. These motors are driven by sets of programming codes encoded in a circuit board assembly switch, channelling the electrical power provided by the 18V Li-OH battery pack. The speed and voltage of the cordless drill used in this study is fixed, only varies by the degree of pressure exerted on the switch.

1.2 Background

In developing cordless electric drills, temperature limits is a key factor affecting the efficiency of the overall performance, differentiating it from the manufacturers' competitions. High temperature is one of the sources of increased stress on cordless impact drills' insulation system, thus cause failures of cordless impact drill. Recognizing the importance of the thermal factor in the overall effectiveness of cordless drill design, different techniques have been proposed for thermal monitoring, in particular those related to the components' temperature. Most of such techniques are based on some intermediate estimates, but in using such techniques little can be said about the distribution of temperature and the identification of thermally critical parts of the tool under the given operating conditions.

1.3 Problem Statement

The development of thermal design methodologies for cordless electric impact drills still is not renowned. The temperature profile and thermal behaviour of components of cordless power tools needs to be further analysed. Furthermore, inefficient and ineffective means of temperature measurement technique for working cordless drill's components give rise to inaccurate review of the temperature rise of the components in the tool.

Figure 1: BOSCH's 18V GDR Cordless Impact Drill will be used as the study equipment

1.4 Objectives

- To determine the temperature profile of selected components on cordless impact drill
- To produce simulation work on temperature profile on the components of cordless impact drill
- To determine the most suitable method of temperature measurement of cordless drill temperature rise test.

1.5 Scope of Study

The project covers both experimental and simulation works. Experiments were done to produce the temperature profile of selected components of the cordless impact drill, varying the materials used and temperature monitoring and measurement methods. The simulation work is done to study and validate the thermal distribution across the components.

1.6 Significance of the Project

The thermal analysis of cordless drill can complement effectively thermal monitoring techniques, contributing significantly to a better understanding of the overall performance and prevention of failures of this cordless drill.

1.7 Feasibility of the Project

The project covers both the experimental work and simulation work. These works (refer to 10.0 Methodology/Project Work) would be feasible in the given 7 months of time allocated with associated constraints and tools available.

CHAPTER 2: LITERATURE REVIEW

2.1 Literature Review

Thermal analyses on modern mechanical machines have been thoroughly studied throughout the past decade. These contribute to fine comprehension of the thermal properties and its applications in the manufacturing industry. This includes large non-portable Numerical Controlled (NC) metal cutting machines, such as the Milling and Lathe machines, to name a few. Thermal analysis on AC electrical machines, using electrical induced motor has also been comprehensively done. However the development of thermal design simulation for cordless electric drills in particular, lags behind.

The following literature review is done to validate the research methodology to achieve the objectives of this research. This critical analysis literature would corroborate three main aspects, namely; the experimental temperature measurement set up, thermal finite element analysis (FEA) and mathematical modelling used to validate the experimental results.

In the matter of temperature measurement set up and thermal FEA, Majumdar et al. (2005), developed a finite element based computational model to determine the temperature distribution in metal cutting processes. The model is based on multi-dimensional steady state heat diffusion equation along with heat losses by convection film coefficients at the surfaces. The temperature inputs were measured directly using two thermocouples in the insert tool.

In line with the above measurement technique, Huai et al. (2002), uses thermocouple heat sensors to validate the mathematical model they develop for the thermal analysis of electric induction motors. Indeed, this report is the closest method

example to be adapted in this study, which also uses electrical induced motor as the main component that drives the cordless drill.

Similarly, Ajiboye and Adeyemi (2007) developed a numerical method to stimulate the non-steady-state temperature distributions during forward extrusion process. On the process, it seems that they agree with Majumdar et al. to use thermocouple as the method to get accurate result for their experimentation.

On the contrary, Abukhshim et al. (2005) critically reviewed previous research on heat generation and heat dissipation in the orthogonal machining process. In addition, the temperature measurement techniques applied in metal cutting are also briefly reviewed. They also studied the relevance of this method, and presented new temperature measurement results obtained by thermal imaging camera of high speed cutting of high strength alloys. They revealed that for High Speed Machining (HSM), tool-work (dynamic) thermocouple only gives a mean value of the temperature along the whole tool-chip interface and high local temperatures which occur for short periods cannot be observed; it gives incorrect results if a built up edge is formed; a coolant cannot be used; both work piece and the tool should be electrical conductors, the thermocouple pair requires accurate calibration and produces significant noise in the signal. In particular, its inability to capture the transient aspects of temperature distribution makes it less ideal for HSM.

Ajiboye and Adeyemi agreed on the first point, where they revealed that the thermal inertia of the thermocouple makes its response to temperature changes to be slow at the early stage of extrusion process. For the alternative, Saglam et al. (2005) used an InGaAs radiation sensor for temperature measurement on the tool tip. Abukhshim et al. believed that the radiation technique (non-contact thermographic methods) has many advantages over the thermo-electric technique including: fast response; no adverse effects on temperatures and materials; no physical contact; and allowing measurements on objects, which are difficult to access. This technique is probably the most suitable in HSM applications where high temperatures can be captured easily as there is no direct contact with the heat source.

In the above review, the experimental temperature measurement set up can be summed up to two main agreements, namely; non-HSM system in favour with thermocouple assembly, and HSM system not in favour with the method. The project is in line with the former, as the cordless drill is not one of HSM system. The proposed method of measurement is to use the thermocouples, despite all its disadvantages in HSM application. In order to test the power tool in actual metal bolting work, the cordless drill must be in complete assembly as designed, in closed housing. Other temperature measurement methods named above, such as the radiation technique will not be effective in measuring the components of the cordless drill located inside the housing assembly.

Furthermore, with regards to above references, all the researchers agrees that simulation of temperature profile done on any part would be most effective using Finite Element Analysis (FEA) to solve governing equations and for the thermal analysis of the components of the desired machine in study.

With regards to the matter, de Filippis S. et al. (2011) clearly express their satisfaction of solving and fully coupled electrical and thermal problem using the FEM method. Simulations and comparison with measurement have been performed in order to validate the simulation approach by means of a test chip. These are done using ANSYS simulator. On that note, L. Benramoul, A. Abdellah El-Hadj concluded a finite element method with ANSYS program is used to solve a set of nonlinear governing equations. In line with the latter, Farinon S. (2007) concluded that ANSYS is thoroughly effective in tackling all the problems that can be typically dealt with a finite element code. It is used to obtain solutions to a large class of engineering problems involving stress analysis, heat transfer, electromagnetism, fluid flow, as well as many coupled field analyses in one, two or three dimensions.

Moreover, after working on an extensive sensitivity analysis, Capriccioli A., and Frosi P., (2009) found that the mechanical calculation results by ANSYS are very sensitive to the mesh shape; this fact implies very fine and regular meshes needed when designing the FEA for this project.

Apart from ANSYS, other FEA software program such as ABAQUS is available to conduct the task of solving mathematical models associated with a finite element analysis. By using ABAQUS, Deng D. and Murakawa H. (2005) employed the finite element models to evaluate the transient temperature and the residual stress fields during welding. Uncoupled thermal–mechanical three-dimensional (3-D) and two-dimensional (2-D) finite element models for SUS304 Stainless Steel pipes were developed. However, as stated by Farinon, to date, the finite element method (FEM) is the most widely used numerical method for solving a variety of problems governed by partial differential equations in all areas of engineering. In particular, ANSYS is a complete finite element analysis (FEA) software package which can be used in virtually all fields of engineering.

In this project, it is proposed that the similar technique used, that is, to use FEA through the software ANSYS in developing the simulation to produce temperature rise profile of the components in the thermal analysis of the cordless drill.

Under the domain of mathematical modelling, it is proposed to use the established mathematical model developed by Huai et al.. The model was designed for thermal analysis of electric induction motors. They had successfully implemented the model, validated it and finally applied the model example. Thus, this model is valid to be applied in this project, where the cordless drill also uses electric induction motor as its main driver, and the main source of heat generation.

2.2 Mathematical Modeling

In this project, the main source of heat as known is the induction motor used in the cordless drill. The following mathematical modelling ultimately reflects how heat is dissipated from the motor during a temperature rise test. The base of the mathematical model Huai et al. developed considered on the following energy balance model:

$$\rho\left(\frac{\partial e}{\partial t} + \mathbf{v}\cdot\nabla e\right) = \boldsymbol{\sigma} : \boldsymbol{\epsilon} - \nabla\cdot\mathbf{q} + \rho Q, \tag{1}$$

where ρ is the density of the material, e is the internal energy, $\mathbf{q}$ is the energy flux, ϵ and σ are deformation and stress tensors, respectively, Q is the energy supply. (1) can be reduced to the following form:

$$\rho\frac{\partial e}{\partial t} + \nabla\cdot\mathbf{q} = \tilde{Q}, \tag{2}$$

where $\tilde{Q} = \rho Q + \boldsymbol{\sigma}^{\boldsymbol{T}} : (\nabla\mathbf{v})$ accounts for the energy supply and changes in the internal energy due to different types of losses, e.g. friction and cooling losses, and electromagnetic losses. Assuming that the internal energy can be expressed as $e = e(\theta)$,

$$\frac{de}{dt} = c_v\frac{d\theta}{dt} \text{ where } c_v = \frac{de}{d\theta}\ , \tag{3}$$

where c_v is the specific heat at constant volume. Model (1)–(3) is supplemented by boundary and initial conditions. Depending on the part of the motor under consideration, Dirichlet's, Neumann's, specified flux, or radiation boundary conditions is used. In doing so, Fourier's law $\mathbf{q} = -k\nabla T$, is used. Newton's law of cooling/heating accounting for convection from the surface $Q_1 = h(T_{ext} - T)$ (heat acquired from the surrounding), and the Stefan–Bolzmann law giving the radiative energy net exchange $Q_2 = C_{cons}\ (T^4_{\text{am}} - T^4)$ (heat acquired due to the incoming radiation), where h is the convection coefficient, T_{ext} and T_{am} are external and ambient temperatures, respectively, k is the thermal conductivity coefficient, and C_{cons} is the radiative transfer coefficient. In this context, it is convenient to introduce a scalar quantity, W_{out}, representing heat losses at the surface. Then, the energy balance at the surface is defined by the formula

$$W_{out} = q_{sup} = k\nabla T - h(T_{ext} - T) - C_{cons}(T^4_{am} - T^4). \quad (4)$$

The representation (4) allows to ‘‘activate’’ coefficients k, h, C_{cons} depending on which specific type of heat transfer (conductive, radiative, or convective) should be accounted for in a particular part of the motor. If the heat generated within the system denoted by W_{in} then the original model can be reformulated as a basic conservation law in the form $W_{out} = W_{in} - W_{change}$ where $W_{change} = \rho c_v \frac{\partial T}{\partial t}$ would formally represent the change in energy stored within the system. In order to complete the model formulation, functions and coefficients entering the model (1)–(4) needed to be specified, since they depend on the geometry and nature of the region of the motor and/or the boundary segment under consideration.

2.2.1 Power Losses In Induction Motors: Heat Sources Modeling

It is well known that experimental techniques aiming at determining total losses and temperature rise in electric induction motors may be expensive, and their effectiveness is often limited to specific types of motors. It is, therefore, often important to estimate analytically or numerically power losses in the motor in order to use the estimates obtained as input parameters for thermal modelling.

Before moving further in modelling heat sources, the fundamentals of the motor considered in this paper will be described. In Figure 2 a photo of an induction motor that is analysed is presented. The motor consists of a shaft, bearing, frame, stator coil, end winding, stator core, rotor, end cap, and a fan.

Figure 2: Cordless Drill induction Motor Analysed

In such motors DC voltages are induced in the rotor circuit by the rotating magnetic field of the stator. When three-phase balanced and symmetric currents are applied to the stator winding, a rotating magnetic flux is produced in the air gap. If the frequency of the applied currents is known, say f , then the speed of the rotating magnetic flux, n_s, can be calculated (in revolutions per minute, rpm) as

$$n_s = 120f/p, \quad (5)$$

where p is the number of poles per phase. The rotating flux in the air gap will induce voltage in the rotor winding, and a current flow in the rotor winding (since the rotor winding circuits are closed). Then, the classical scheme applies: the current in the rotor winding will interact with the rotating magnetic field in the air gap, and a Lorentz force will be produced and act on rotor conductors $\mathbf{F} = q\mathbf{v} \times \mathbf{B}$, where q is a charge moving through an external magnetic field **B** with velocity **v**. As a result of this force, a torque is produced and the rotor assembly starts rotating. As it is well known, the requirement for the torque to be produced in the motor the actual mechanical rotating speed of the rotor should be less than the speed of the rotating magnetic flux produced by the stator. The difference in rotating speeds between the stator produced magnetic flux and the rotor is measured by the slip

$$s = n_s - n / n_s \quad (6)$$

where n is the rotor speed in rpm. When a motor is used to drive the load connected on its shaft, it inevitably encounters losses, which serve as heat sources distributed throughout the whole motor and vary with different operating conditions. To account for the total losses is an extremely difficult task, but it is possible to divide all motor power losses into five major categories:

- stator core losses (iron losses, denoted further by P_m);
- stator coil losses (copper losses, denoted further by P_{cu1});
- rotor coil losses (copper losses, denoted further by P_{cu1});
- friction and windage losses (mechanical losses);
- stray load losses.

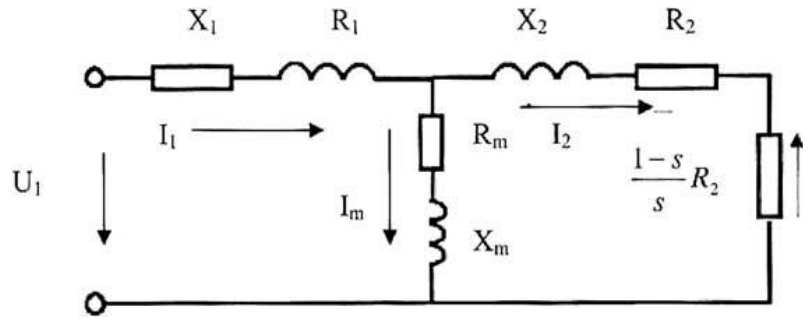

Figure 3: The equivalent circuit of an induction motor used in calculation of losses

Given the supply frequency, ω, it is possible to approximate the power losses by experimentally fitted dependency

$$P_{\text{losses}} = F(\omega), \tag{7}$$

where it is often appropriate to use a cubic polynomial in place of F , e.g. $P_{\text{losses}} = a_0 + a_1\omega + a_2\omega^2 + a_3\omega^3$. However, it is important to emphasize that the distribution of losses in different parts of the motor could be substantially different. Therefore, in the general case approximation (7) has to be replaced by a more rigorous technique for the evaluation of power losses.

The estimates of friction losses usually account for a small part of the total losses, but when the speed increases, their contribution should be included, in particular in the air gap, end rings, rotor ends, shaft and bearing. It is known that the first three categories of losses mentioned above (generically known as electromagnetic losses) account for 75–90% percent of the overall losses. Therefore, in what follows it is focused on the evaluation of these electromagnetic losses which can contribute substantially to the temperature distribution in the motor.

Different methodologies exist to deal with different aspects related to the electromagnetic losses evaluation. Here, a more classical approach based on the equivalent circuit methodology is used. The induction motor equivalent circuit model, shown in Figure 2, is constructed by using the following set of induction motor parameters: (R_1, $X_{1\sigma}$), (R_m, X_m), and (R_2, $X_{2\sigma}$). Each pair represents resistance and

leakage reactance, respectively. The first pair deals with the stator parameters, while the third one deals with the rotor. The second pair of parameters takes care of magnetizing effects and models the generation of the air gap flux within the induction motor. The importance of this pair increases when the induction motor is driven with voltages other than the rated supply voltage and frequency due to the fact that under operation with a variable voltage and/or variable frequency the induction motor could saturate if the stator voltage is excessively large. Other parameters of interest presented in Figure 2 are U_1 (per-phase supply voltage of the stator) and I_1, I_m, I_2 (the phase currents of stator, magnetizing and rotor circuit, respectively). These parameters can vary in the model with different operational conditions. By using the standard equivalent scheme technique, Ohm's law is applied, and the required electromagnetic losses are calculated as follows:

$P_{cu1} = mR_1{I_1}^1$ (stator copper losses), (8)

$P_m = mR_m{I_m}^2$ (stator core losses), (9)

$P_{cu2} = mR_2{I_2}^2$ (rotor copper losses), (10)

where m is the phase number of the motor. Formulae (8)–(10) are used with the values for the phase currents computed by

$$I_1 = \frac{U_1(Z_m+Z_2)}{Z_{1\sigma}Z_m+Z_{1\sigma}Z_2+Z_mZ_2}, \quad (11)$$

$$I_2 = \frac{U_1Z_m}{Z_{1\sigma}Z_m+Z_{1\sigma}Z_2+Z_mZ_2}, \quad (12)$$

$$I_m = \frac{U_1Z_2}{Z_{1\sigma}Z_m+Z_{1\sigma}Z_2+Z_mZ_2}, \quad (13)$$

where $Z_{1\sigma}$, Z_m and Z_2 are the phase impedance of stator, magnetising and rotor circuit, respectively.

$Z_{1\sigma} = R_1 + jX_{1\sigma}$, $Z_2 = R_2/s + jX_{2\sigma}$, $Z_m = R_m + jX_m$. (14)

Finally, the leakage reactances $X_{1\sigma}$, $X_{2\sigma}$ and X_{m} entering (14) are computed by using the following formulae

$$X_{1\sigma} = 2\pi f l_1,\ X_{2\sigma} = 2\pi f l_2,\ X_{\mathrm{m}} = 2\pi f l_m, \tag{15}$$

where l_{i}, i = 1, 2, 3 are leakage inductances of stator and rotor, and the magnetized inductance, respectively. The values of these parameters are assigned when the motor is designed. The next task is to evaluate heat transfer mechanism parameters. All three main transfer mechanisms, conduction, radiation, and convection, are involved in the heat exchange in the motor.

2.2.2 Heat Transfer In Induction Motors Via Conduction And Radiation

In the solid parts of motors, such as the rotor and stator, heat is typically transferred by conduction. Hence, for these parts the standard Fourier's law to connect the heat flux and the temperature gradient is used:

$$q = -k\nabla T \tag{16}$$

A part of heat in induction motors is transferred by radiation. The actual amount of energy transferred in the form of electromagnetic waves depends not only on the emissivity properties of the part of the motor under consideration, but also on the temperature itself in a strongly nonlinear way. Due to a temperature difference between the motor surface and the ambient temperature, the heat will be radiated out from the whole of the motor surface, and the energy radiated can be evaluated according to the Stefan–Boltzmann law of radiation:

$$Q = \epsilon\sigma T^4 A\Delta t, \tag{17}$$

where A is the surface area of the motor under consideration, ϵ is the emissivity coefficient, and σ = 5.67 x 10^{-8} W/m^2**K**^{4} is the Stefan–Boltzmann constant. In the notation used before $C_{\mathrm{cons}} = \epsilon\sigma$. In the most general setting, accounting for electromagnetic radiation should lead to an integro-differential due to the fact that electromagnetic radiation propagates in all directions. However, if the diffusion

approximation is used the discussion on heat exchange can be reduced formally to conductive Fourier's law $\mathbf{q} = -k_r \nabla T$, but with strongly temperature-dependent radiative coefficient, $k_r = 16\sigma/(3\kappa_r)$, where κ_r is the Rossseland mean absorption coefficient. As discussed in the next section, a similar expression can also be used for the convection, but the estimation of the heat transfer coefficient in that case is conducted in a quite different manner.

2.2.3 Heat Transfer In Induction Motors Via Conduction

In evaluating the convection coefficient h for the heat transfer from the frame to the external environment, the dissipation from the fins of the frame (denoted further by h_a) and the dissipation from the surface between the fins (denoted further by h_l) must be taken into account. The evaluation of these coefficients is complex, and in the general case the values of these coefficients vary depending on (a) the spatial position (due to the airflow losses on the frame), and (b) the airflow characteristics provided by the external fan. A method for calculating the forced convection coefficient depending on the Reynolds number is described here:

$$Re = V_a F_l / \kappa \tag{18}$$

where V_a is the airflow velocity at beginning of the fins (it is known that this velocity is approximately 70% of the peripheral fan speed, obtained from experimental results), F_l is the axial length of the fins, and κ is the kinematic viscosity of the air.

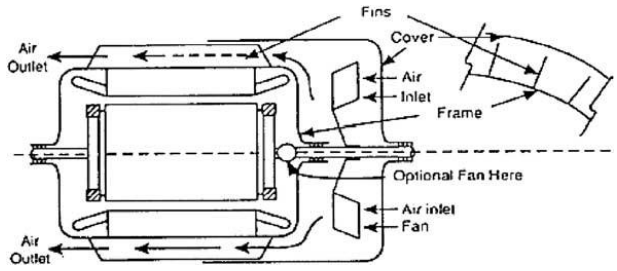

Figure 4: Cooling airflow paths of the induction motor

The general procedure for the evaluation of h_a and h_l which requires an estimate for (18), after which the procedure follows one of the following two directions.

Laminar airflow case (Re < 7 x 10^4):

In this case the quantity is defined as:

$$H' = \frac{0.7(Re)^{0.5}[1 - 0.12\left(\frac{F_h}{F_w}\right)^{\frac{1}{3}}]K}{F_1} \quad , \tag{19}$$

where F_w is the distance between two fins and F_h is the height of the fins, and K is the thermal conductivity of the air. Then, the convection coefficient related to the dissipation from the fins of the frame is calculated as follows:

$$h_a = H'[1 - 0.02(F_h/F_w)], \tag{20}$$

and the value of convection coefficient related to the dissipation from the surface between the fins as

$$H' = \frac{0.7(Re)^{0.5}[1 - 0.35\left(\frac{F_h}{F_w}\right)^{0.5}]K}{F_1} \quad , \tag{21}$$

Turbulent airflow case (Re < 7 x 10^4):

In this case, H' is calculated as

$$H' = \frac{0.035(Re)^{0.6}[1 - 0.09\left(\frac{F_h}{F_w}\right)^{0.5}]K}{F_1} \quad , \tag{22}$$

By using the value (22), h_a is then calculated according to formula (20), while for the calculation of h_l the following formula is used

$$H' = \frac{0.03(Re)^{0.8}[1 - 0.23\left(\frac{F_h}{F_w}\right)^{0.5}]K}{F_1} \quad , \tag{23}$$

Finally, the free convection coefficient noted by using the following formula

$$h_{free} = 6.5 + 0.05(T - T_{ext}). \tag{24}$$

Now, the project is in a position to describe the main steps of the computational procedure.

CHAPTER 3: METHODOLOGY/PROJECT WORK

2.1 Research Methodology

After having the literature review and the mathematical modelling done, the outline of the research methodology is decided as follows (Flowchart as attached in Appendices):

- Conception of established mathematical modelling
- Acquiring necessary materials, tools and equipments needed
- Experimentation of metal bolting using thermocouples and data logger.
- Temperature profile of components of cordless impact drill using different temperature measurement methods and different materials.
- Simulation of the temperature distribution for the tool component using ANSYS by means of Finite-Element Analysis (FEA)
- Discussion/Analysis/Conclusion.

2.2 Equipments

- 18V Cordless drill
- units 18V Battery packs
- 8 Thermocouple coupled with data logger
- ANSYS Mechanical APDL Software
- 20.0mm (T) x 230.0mm (W) x 0.34mm (L) Steel Plate, and Jelutong Wood
- 20 x 16mm steel bolts, nuts and washers
- Personal Computer
- FL Infra Red Thermo graphic Camera and its components

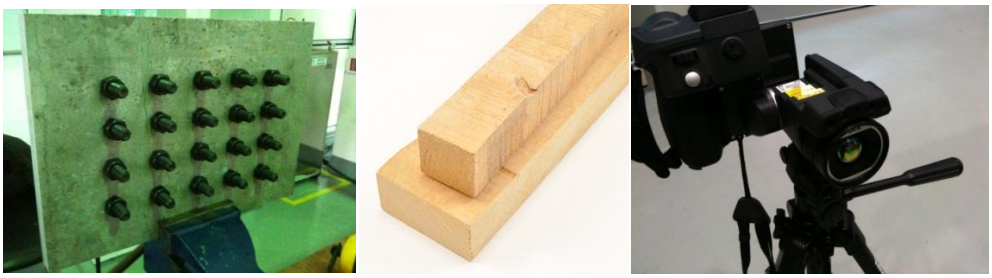

Figure 5: (a) Steel Plate with mounted bolts, nuts and washers, (b) Jelutong wood block and (c) Infrared Thermographic camera

3.3 Temperature Rise Experimental Procedure

1. battery packs are fully charged before the experimentation
2. 20 metal bolts, nuts and washers were mounted onto a pre-drilled 20 holes' steel plate (Figure 5(a))
3. Using hard glue, 8 thermocouples were attached at 8 different measurement locations on the cordless impact drill as shown in the Figure 7 to Figure 14.
4. Data logger's data measurement time interval was set.
5. The temperature recording of the components of the cordless impact drill was started.
6. By following a 3 seconds bolting, 2 seconds rest routine, metal bolting experiment was started and continuously repeating the routine to exhaust the first battery pack. The temperature measurement recording was not stopped.
7. After exhausting the first battery pack, two minutes rest was given and continue to bolt with the second fully charged battery pack, and exhausting it.
8. 7 minutes was given for rest.
9. The temperature recording was stopped.
10. This procedure is repeated for wood bolting set up, using a self-tapping screw to bolt into Jelutong wood, to exhaust 2 battery packs.
11. The procedure is repeated again for metal bolting using infrared thermo graphic camera to measure the surface temperature of the cordless impact drill, thus validating the simulation on the transient thermal distribution.

12. The temperature profile of metal bolting and wood bolting were plotted and infra red thermo graphic images were analysed for further discussion.

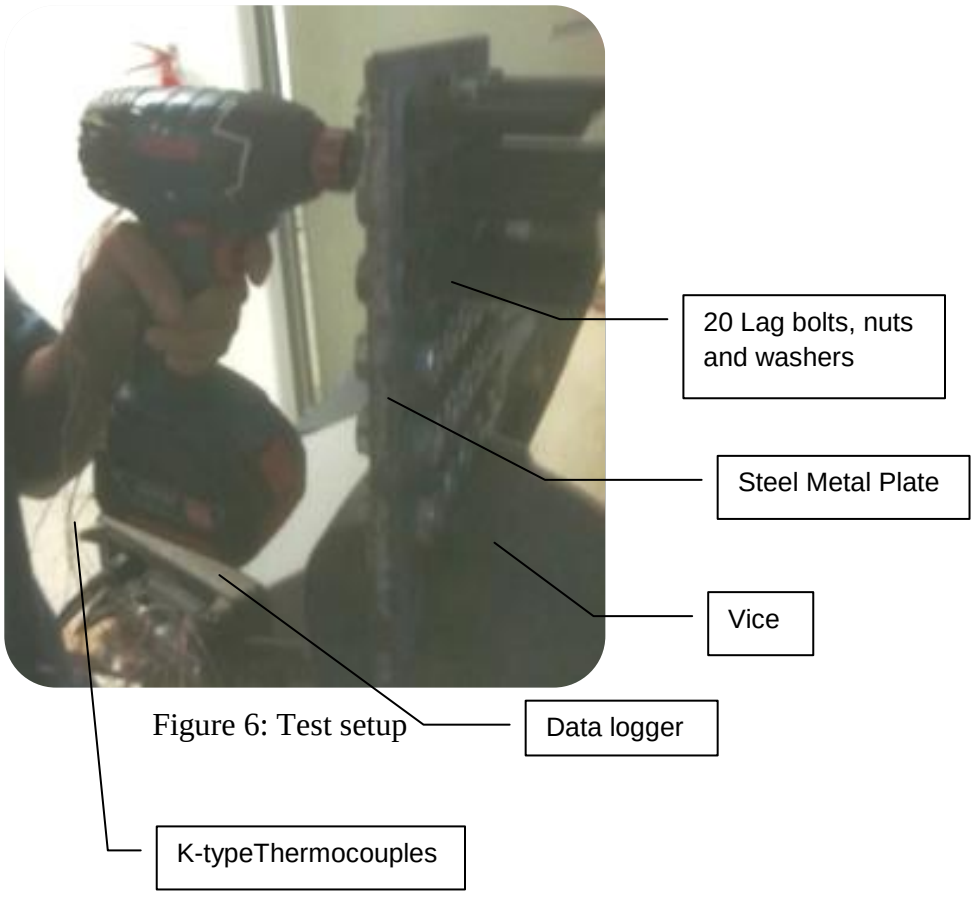

Figure 6: Test setup

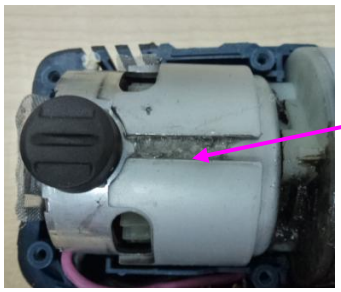

Figure 7: Motor Can measurement location

Figure 8: Internal Gearbox measurement location

Figure 9: MOSFET measurement location

Figure 10: External gearbox measurement location

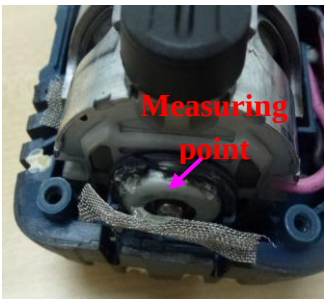

Figure 11: End bell measurement location

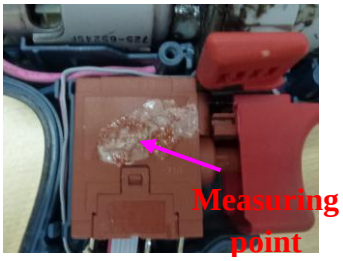

Figure 12: Switch measurement location

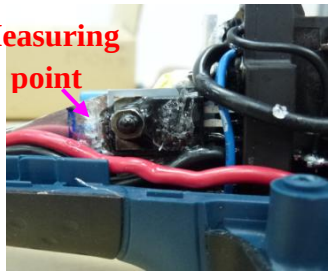

Figure 13: Heat sink measurement location

Figure 14: Handle measurement location

CHAPTER 4: RESULTS & DISCUSSION

4.1 Results

4.1.1 Tabulation of Results and Temperature Profile

Table 1: Tool information

Type Label
Rated Voltage:18V
Rated Current: N/A
Rated RPM:0- 2800min-1

Table 2: Battery Pack and Wood Information

	Information	Battery label	
		Battery 1	Battery 2
18V Metal Bolting TR1	Full charged voltage	20.88 V	20.89 V
	Depleted voltage	15.19 V	15.15 V
	Capacity performance	226	166
18V Wood TR1	Full charged voltage	20.89 V	20.92 V
	Depleted voltage	15.56 V	15.71 V
	Wood density	440kg/m³	444kg/m³
	Capacity performance	90 holes	96 holes

Table 3: Data Tabulation for Metal and Wood Bolting Temperature Rise Experiment

No	Thermocouple Location	Temp. Limit	TR1 Metal bolting		TR1 Wood	
			Max. Temp. (ºC)	Temp. Rise (K)	Max. Temp. (ºC)	Temp. Rise (K)
1	Motor(C)	<100ºC	116.86	91.86	90.28	65.28
2	End Bell(C)	<100ºC	114.91	89.91	80.94	55.94
3	Internal Gearbox(C)	N/A	131.72	106.72	105.23	80.23
4	Switch(C)	<65ºC	70.38	45.38	45.39	20.39
5	Mosfet(C)	<100ºC	51.10	26.10	42.11	17.11
6	Heat sink(C)	<100ºC	49.92	24.92	41.93	16.93
7	External Gearbox(C)	<100ºC	98.42	73.42	76.61	51.61
8	Ambinet(C)	N/A	25.00	0.00	25.00	0.00
9	Handle(C)	⌂<20K	46.52	21.52	38.72	13.72

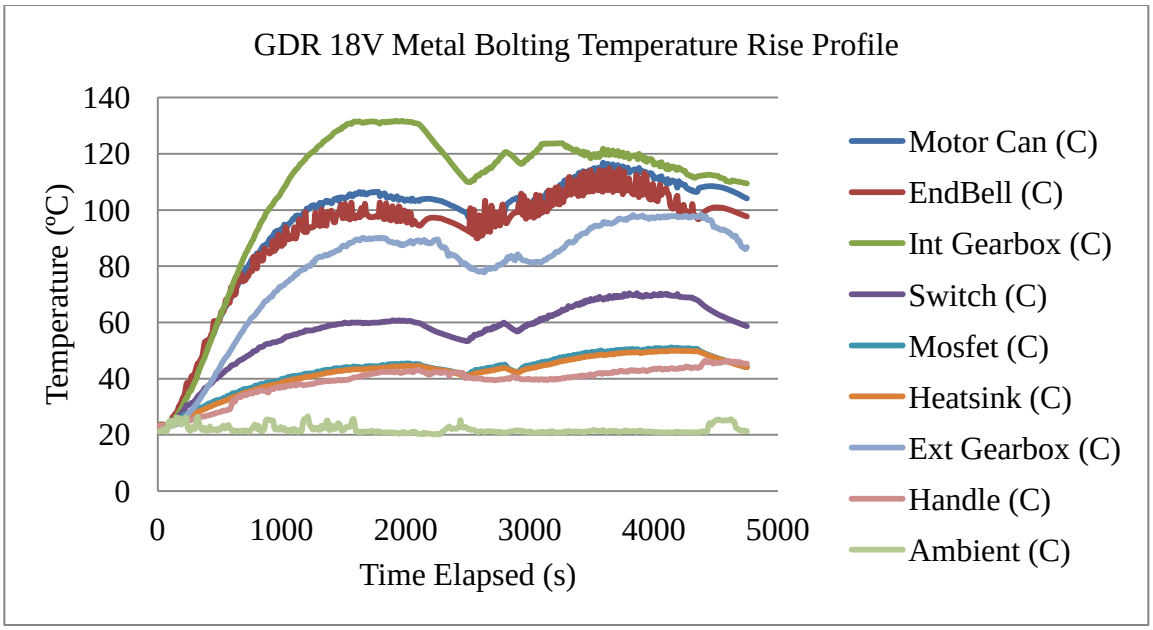

Figure 15: GDR 18V Metal Bolting Temperature Rise Profile

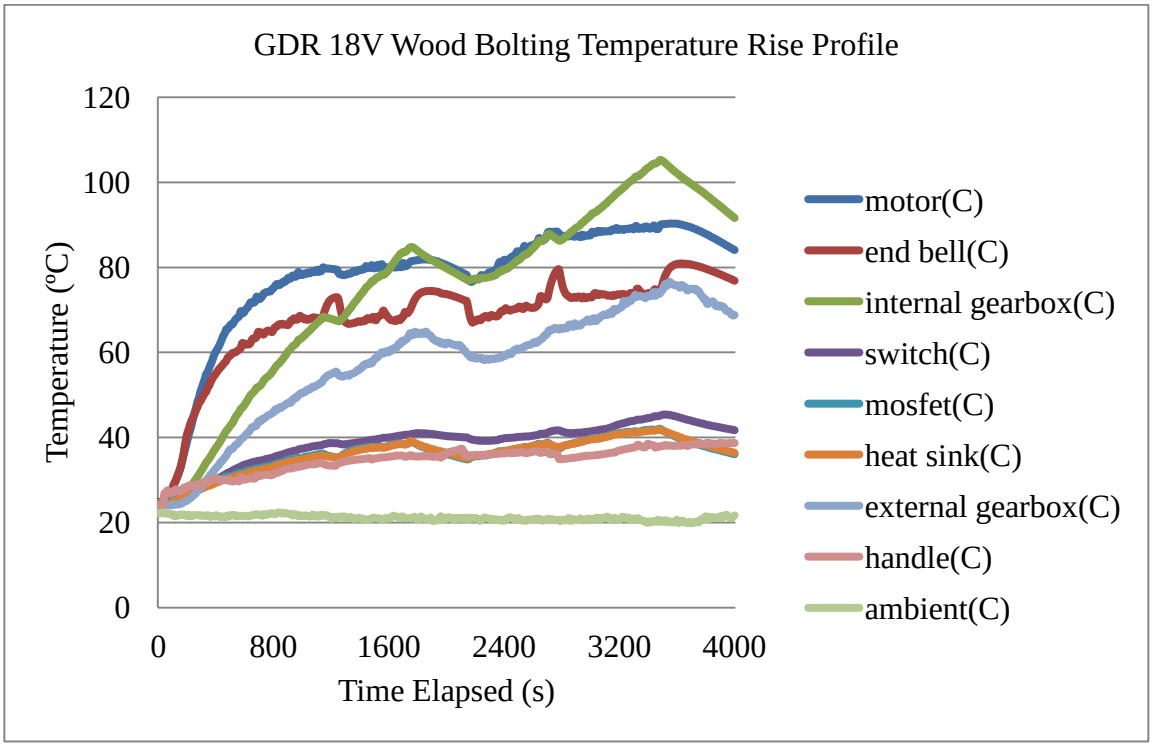

Figure 16: GDR 18V Wood Bolting Temperature Rise Profile

4.1.2 Temperature Distribution Simulation

As being explained in the literature review, on the induction motor, Huai et al. have developed the following for the induction motor:

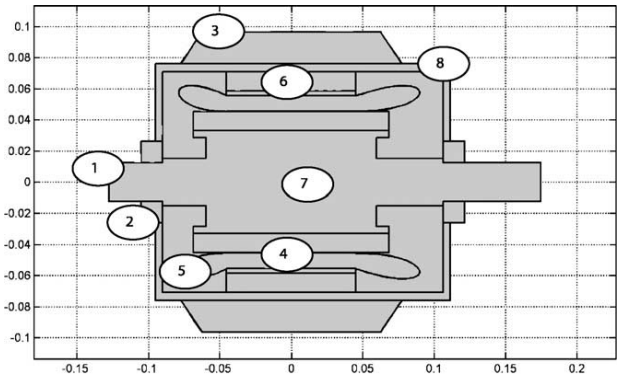

Figure 17: The axial cross-section geometric configuration of the motor.

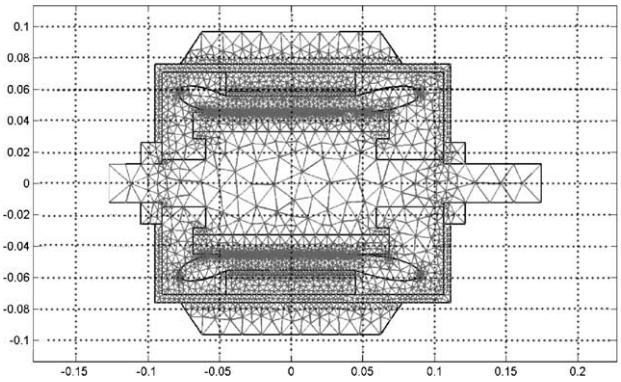

Figure 18: Finite element discretisation grid generation.

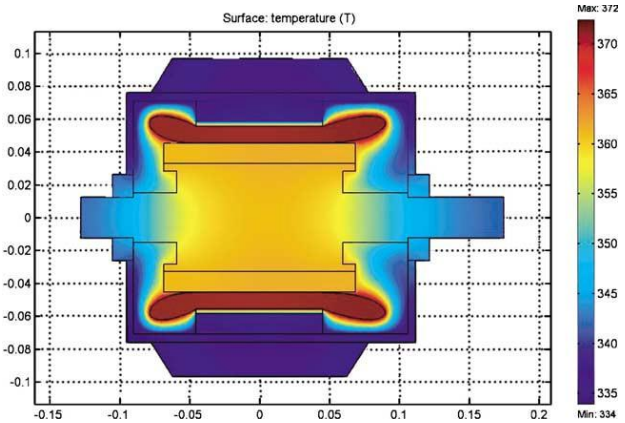

Figure 19: Typical temperature distribution in the axial cross-section of the motor.

Thus, to simulate the thermal distribution across the tool housing, the following have been done:

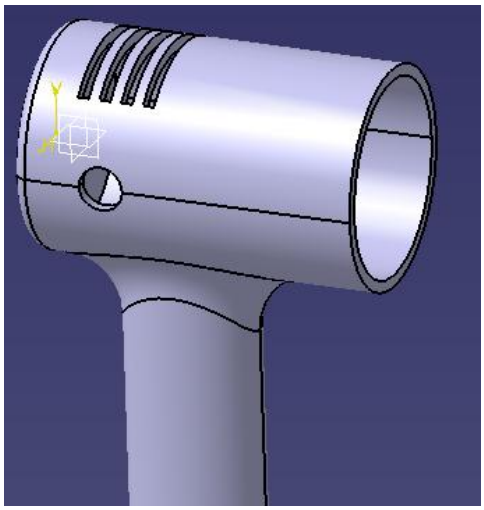

Figure 20: GDR 18V Catia V5 Housing Drawing

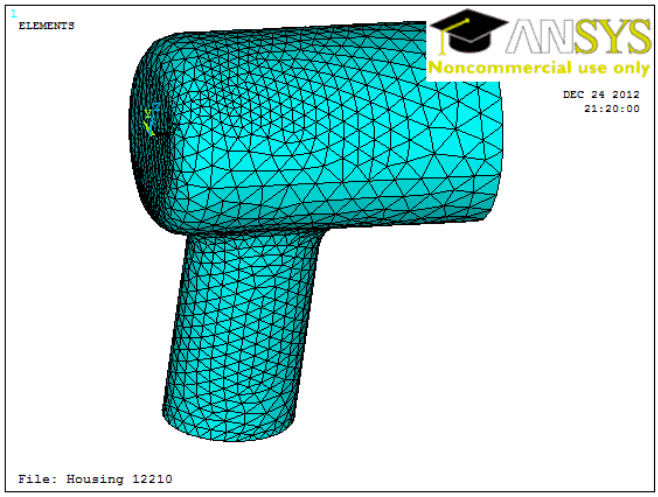

Figure 21: GDR 18V Housing Finite Element discretisation for FEA Heat Transient Analysis

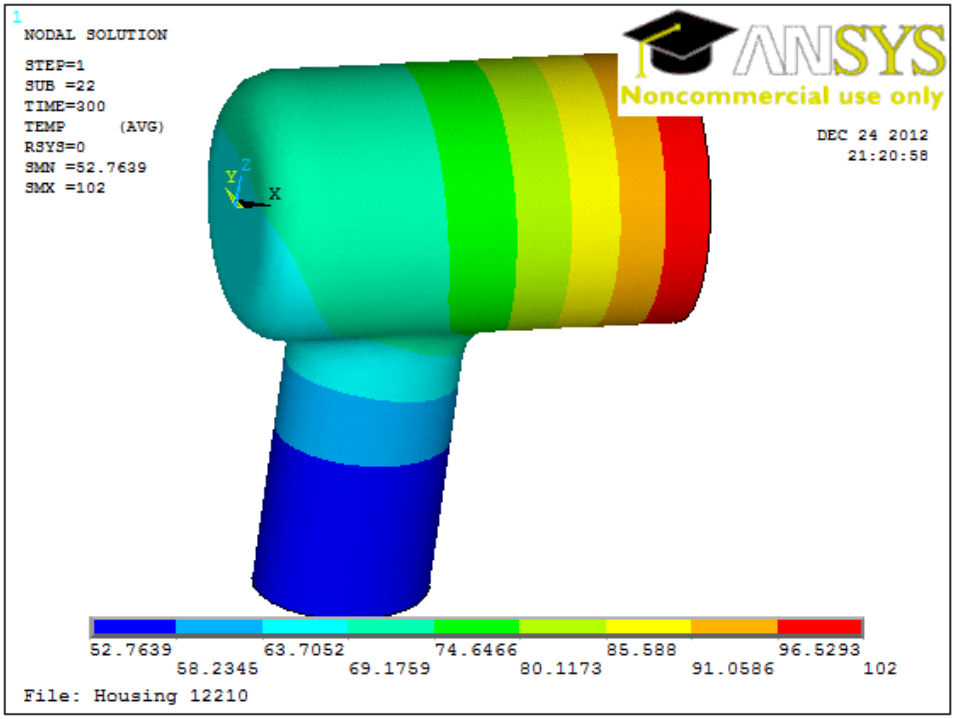

Figure 22: ANSYS Thermal Transient Simulation

4.1.3 Temperature measurement method

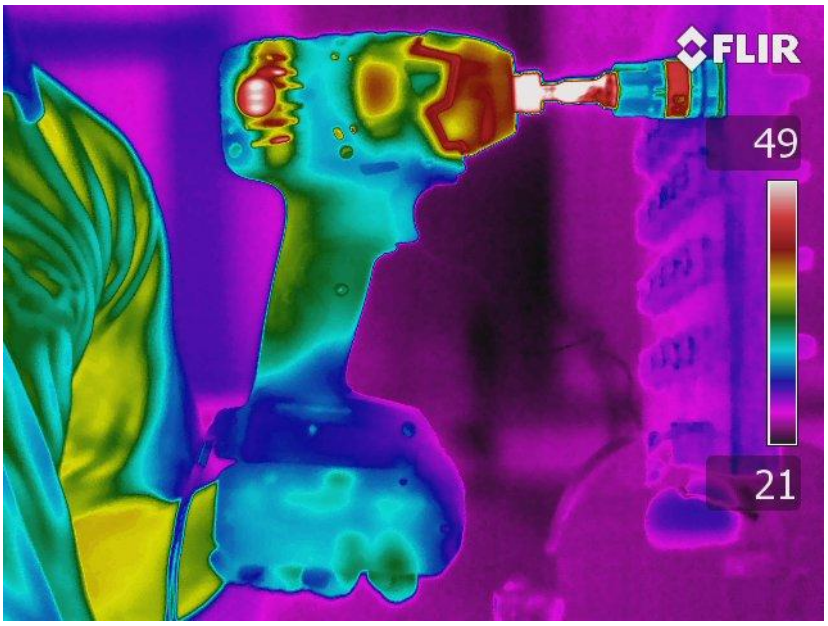

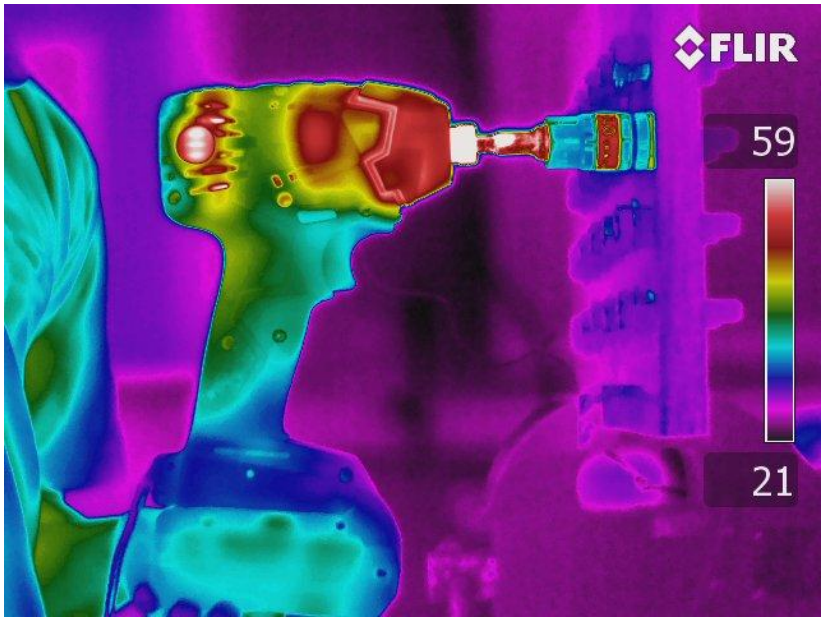

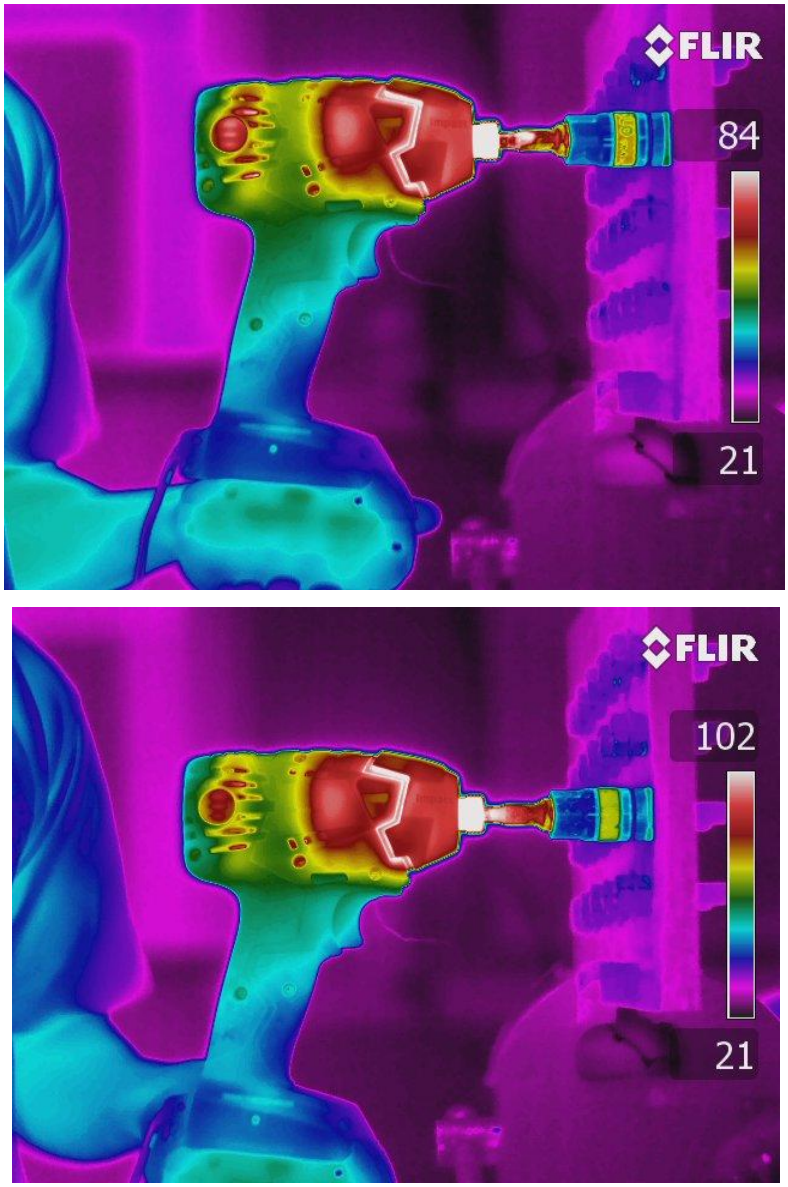

Figure 23: Infrared Thermo graph images of the metal bolting temperature rise test

Finding: The usage of thermocouple assembly is seen to be the most reliable and accurate mean of cordless drill internal components' temperature measurement, while thermo graphic imaging is accurate for surface temperatures.

4.2 Discussion and Analysis

The type of thermocouple used in the experiment is type K (Nickel-Chromium / Nickel-Alumel). The type K is the most common type of thermocouple. It's inexpensive, accurate, reliable, and has a wide temperature range. The temperature measurement point is a vital aspect of this project. Thus, 8 K-type thermocouples are attached to 8 different points on the cordless impact drill.

The 1st measuring point is the motor can. This is the most important point, as it serves as the root cause related to tool failure with regards to temperature rise. The high temperatures of the armature and stator may melt and cause disturbance on the electromagnetic flux generated, causing less electrical energy converted to kinetic energy, thus loses RPM and power. As been explained in Chapter 2 (Literature Review), the thermal behaviour of the interior parts of the motor has been thoroughly studied by Huai et al. They also proposed and proved the mathematical modelling that explains the heat dissipation by 3-phase induction motor inside out. Thus, in this project, it is sufficient just to measure the outer part of the motor can to measure the motor temperature.

The 2nd measuring point is the internal gearbox. As seen in the test results, the internal gearbox temperature clearly controls the thermal transient across the tool, as it exhibits the highest temperature range of the tool. However, in cordless drill industry, gearbox's high temperature very seldom poses threat to the tool life, and user, as it is well insulated by the elastomers, and the components inside the gearbox (gears and clutch) can withstand very high temperatures without degrading its life very fast.

The 3rd measurement point is on the MOSFET. Acronym for metal-oxide semiconductor field-effect transistor, MOSFET is used for amplifying or switching electronic signals. It is a vital part of the cordless drill electronics. Thus monitoring its temperature in this test is important.

Next, the 4th measurement point is the end bell measurement location, located at the back of the motor. This is where a user usually places his hand to support the bolting work. The 5th temperature measurement point is the switch, where vital electronics are located to translate the pressure exerted on the switch to the power of the tool itself. The 6th point is the last point heat dissipates before reaching the MOSFET, printed circuit board assembly and the batteries; the heat sink.

The 7th and 8th measurement points, located at the external gearbox and handle respectively, purposely measured for the benefit of professional user's comfort while using the cordless power tool at work.

Two battery packs was used to run this test. The purpose of providing two battery packs is simply because in a tight schedule of a professional user, the impact drill is used continuously to get his work done. Thus, while charging up an exhausted battery pack, the user can continue his work with another battery. The usual rest time in between the two battery pack is 2 minutes, relieving his arms from the vigorous vibration of the process. The continuous repetitive 3 seconds bolting and followed by 2 seconds rest routine is the average bolting time and routine usually applied by professional users. Therefore, the test procedure itself is actually the simulation of the real life situation for the usage of 18V cordless impact electric drill in the industry by professional users.

Figure 15 and Figure 16 shows the temperature-time graph profile of the test. This test determines if the temperature rise of components of the tool is within the set limits when the tool is used for metal bolting to exhaust two battery packs. The drop in the middle of the graph is the 2 minute period when the first battery pack is replaced with the fully charged second pack. It was revealed in this test, that the main source of heat generation is from the gearbox. It can be inferred to, that the heat dissipated from the gearbox is produced by frictional forces.

In this graph, the main concern is the temperature of the motor. 100 º C limit is the test requirement for the motor when the cordless tool used in work straight with 2

battery packs. Exceeding this temperature means hazard to the user, and the device. However, the test conducted proves that the motor and the tool are functioning well despite the high temperatures. Additionally, cooling and air-ventilation takes place, thus help to reduce and maintain the motor's temperature.

The graph differs between metal bolting and wood bolting is generally depending on the hardness of the material being used for the bolting work, as well as the test procedure. The wood used in this test is Jelutong wood. In Malaysia, Jelutong is regarded as soft wood, which can be sculptured for various ornaments and household utensils. The bolting in this material uses self tapping screw as shown in Figure 24.

Figure 24: Self Tapping Hexagon head screw

Therefore, the temperature profile is different from metal bolting test, which the user bolts into pre-drilled metal plate continuously following the routine. This is because; cordless impact drill is not designed for steel drill, and is designed for wood drill. From the explanation, it can be inferred to that more heat is generated both from the gearbox and the motor from the impact effect on different hardness of the material, tightening bolts in steel plate as compared to that of penetrating self tapping screw into a Jelutong wood block. Nonetheless, the temperature measurement setup for both metal bolting and wood bolting is exactly the same, thus is valid for comparison and analyzed on the same basis.

The simulation of temperature distribution across the tool surface is done to simulate theoretically the temperature distribution across the surface, by means of Finite Element Analysis. However, with the limited license the university have, only primitive shapes as been designed in the simulation can be meshed by the software (32,000 nodes is the maximum node number able to be meshed). By the input of thermal parameters

persist to the actual material of the tool housing such as specific heat capacity and density, this method also allows the actual temperature profile and thermo graph imaging to be validated. Likewise, the thermo graph image also validates the simulation as shown in figure below. Taking 102 ºC (gearbox temperature) as the reference point, it can be seen that the thermal transient across the tool housing is about similar for both actual and simulation. It can be seen that the handle temperature below (marked with black dot), for both actual and simulation is in the same range of temperature, 60-70º C.

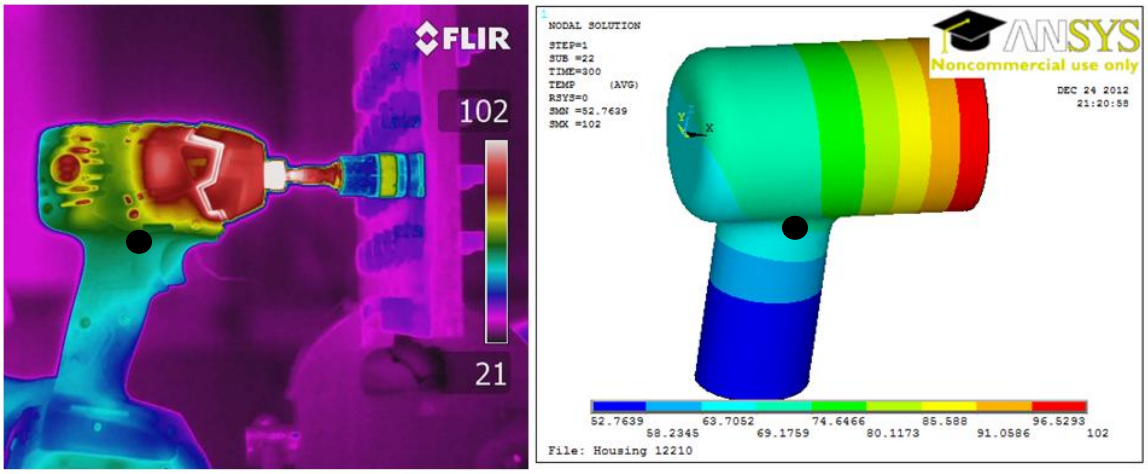

Figure 25: ANSYS Thermal Transient simulation across the housing compared to the actual metal bolting thermo graph image

The infrared thermo graphic camera temperature measurement of the surface of the tool was seen to be sensitive and accurate for surface temperature measurement, when compared to the data recorded with thermocouple assembly.

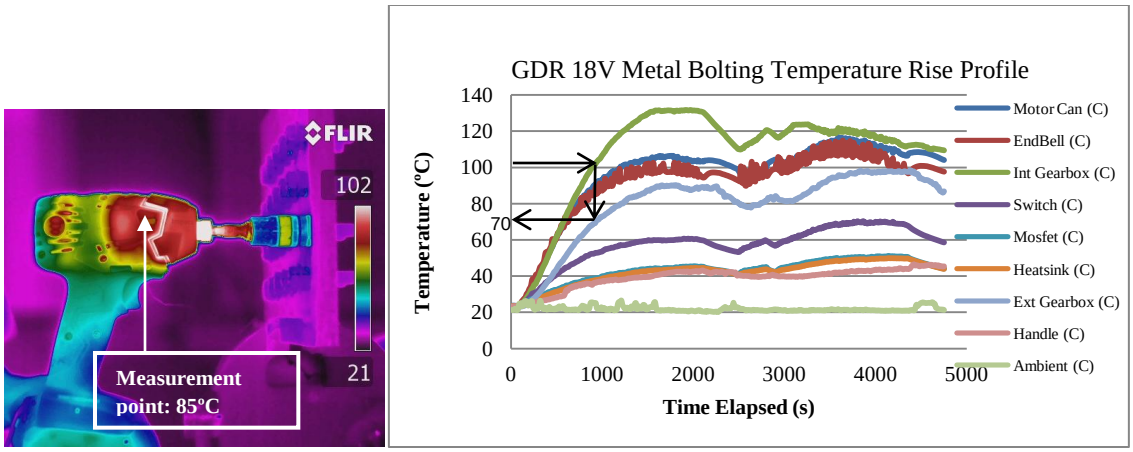

Figure 26: Thermograph surface temperature measurement compared to thermocouple surface measurement

The above comparison is to prove and validate the accuracy and sensitivity of the Infrared thermograph image of surface temperature measurement as compared to thermocouple assembly, at 102ºC gearbox temperature. Following the black arrows on the temperature profile, it can be observed that the surface temperature of the external gearbox using thermocouple assembly is in the range of 70ºC, while the thermo graph camera capture the same point to be in the range of 85ºC.

However, the comparison above cannot be regarded very accurate. This is because the tests using thermocouple assembly and thermograph imaging was conducted at different times, different locations and different environment. However, the tool, equipments and procedure for both experiments conducted were completely the same, except for the different thermocouple and data logger facility. 3-points thermocouples coupled with a data logger is being used while the thermograph imaging is done. Throughout the process, the temperature recorded on the screen of the data logger is continuously being monitored as shown in Figure 27 to observe the accuracy of the thermograph images, and it was proven so.

Figure 27: Data logger screen monitored

Nevertheless, in order to test the power tool in actual bolting work, the cordless drill must be in complete assembly as designed, in closed housing. Other temperature measurement than thermocouple, methods such as the infrared radiation measurement technique will not be effective in measuring the components of the cordless drill located inside the housing assembly. As seen in Figure 23, one cannot measure the specific temperature of the internal vital components of the tool.

On that note, measuring the tool's internal components in an open housing would surely be inaccurate, as the thermal energy will dissipate into the surrounding, thus leaving the components cooler than in actual bolting work. Internal components includes the motor, end bell, internal gearbox, MOSFET, heat sink and switch, while external surface measurement includes external gearbox and handle temperatures.

It can be concluded that, having both methods being used together would be the best solution to measure both the surface temperature of the housing, and the temperature of the internal components for thermal transient study on the cordless impact drill.

CHAPTER 5: CONCLUSION & RECOMMENDATIONS

5.1 Conclusion

This project successfully proposed a general approach to modeling temperature rise phenomena in cordless impact drill, and demonstrated the thermal transient and distribution across the tool from the heat source.

The approach is to conduct a temperature rise test using different temperature measurement methods and materials, followed by a simulation true to the actual constrains, conditions and parameters to the actual tool by using multiphysics analyzer software, ANSYS.

In this project, the temperature profiles of selected components (Motor can, internal gearbox, MOSFET, heat sink, end bell, switch, external gearbox and handle) of a cordless impact drill have been successfully produced. The simulation work on the thermal distribution of the component of the tool has been studied and finally the most suitable and accurate temperature measurement methods have been identified.

In the current Power Tools market, cordless impact drill technology and advancement is on the race. The approach might be very primitive now, as many more measures can be done to over the whole sphere of transient heat study of cordless impact drill. This project would serve as the stepping stone on further thermal research for the benefit of cordless impact drill industry in the future.

5.2 Recommendations

More research on the failure analysis of motor affecting both the circuit assembly and user must be done involving different methods and materials such as concrete and hard wood (eg: Meranti, Chengal, and Pine Wood) to study and validate the root cause of cordless impact drill failures in the industry.

The usage of Mechanical APDL ANSYS 14 software helps a lot researcher to understand the thermal transient and behaviour of the tool housing. When solved, various thermal data and analysis were produced such as thermal heat flux, and heat energy dissipation. These can be further studied in continuing this research.

The modelling of the housing can be made more precise with a higher level license of the software. Even the actual drawing of the housing can be imported if the software can support heavier input, thus producing higher accuracy of simulation of thermal transient across the cordless impact drill.

Other than that, it is also recommended that when conducting metal bolting or wood bolting, both temperature measurement techniques is done simultaneously, and temperature profile can be plotted against time. This step is important so as to verify the accuracy of test data in real time.

Finally, it is also recommended that various other means of temperature measurement techniques is explored specifically to measure cordless impact drill's internal and external components, other than thermocouple assembly and Infrared thermograph imaging.

REFERENCES

Abukhshim N. A., Mativenga P.T., Sheikh M.A. (2005). Heat generation and temperature prediction in metal cutting: A review and implications for high speed machining. International Journal of Machine Tools & Manufacture , 46, 782–800.

Ajiboye J.S., Adeyemi M.B. (2007). Effects of extrusion variables on temperature distribution in axisymmetric extrusion process. International Journal of Mechanical Sciences , 50, 522–537.

Benramoul L., El-Hadj A.A. (2011). An elastic-perfectly plastic model for simulating an aluminum particle behavior during plasma thermal spraying using the finite element method. Applied Surface Science , 258, 962-971.

Capriccioli A., Frosi P. (2009). Multipurpose ANSYS FE procedure for welding processes simulation. Fusion Engineering and Design , 84, 546-553.

De Filippis S., Kosel V., Dibra D., Decker S., Koeck H., Irace A. (2011). ANSYS based 3D electro-thermal simulations for the evaluation of power MOSFETs robustness. Microelectronics Reliability , 51, 1954-1958.

Deng D., Murakawa H. (2005). Numerical simulation of temperature field and residual stress in multi-pass welds in stainless steel pipe and comparison with experimental measurements. Computational Materials Science , 37, 269-277.

Farinon, S. (2007). Magnet design and optimization: The INFN-Genova experience using ANSYS. Cryogenics , 47, 577-582.

Huai Y., Melnik R.V.N., Thogersen P.B. (2002). Computational analysis of temperature rise phenomena in electric induction motors. Applied Thermal Engineering , 23, 779–795.

Majumdar P., Jayaramachandran R., Ganesan S. (2005). Finite element analysis of temperature rise in metal cutting processes. Applied Thermal Engineering , 25, 2152–2168.

Saglam H., Unsacar F., Yaldiz S. (2005). Investigation of the effect of rake angle and approaching angle on main cutting force and tool tip temperature. International Journal of Machine Tools & Manufacture , 46, 132–141.

APPENDICES

A) Methodology flowchart

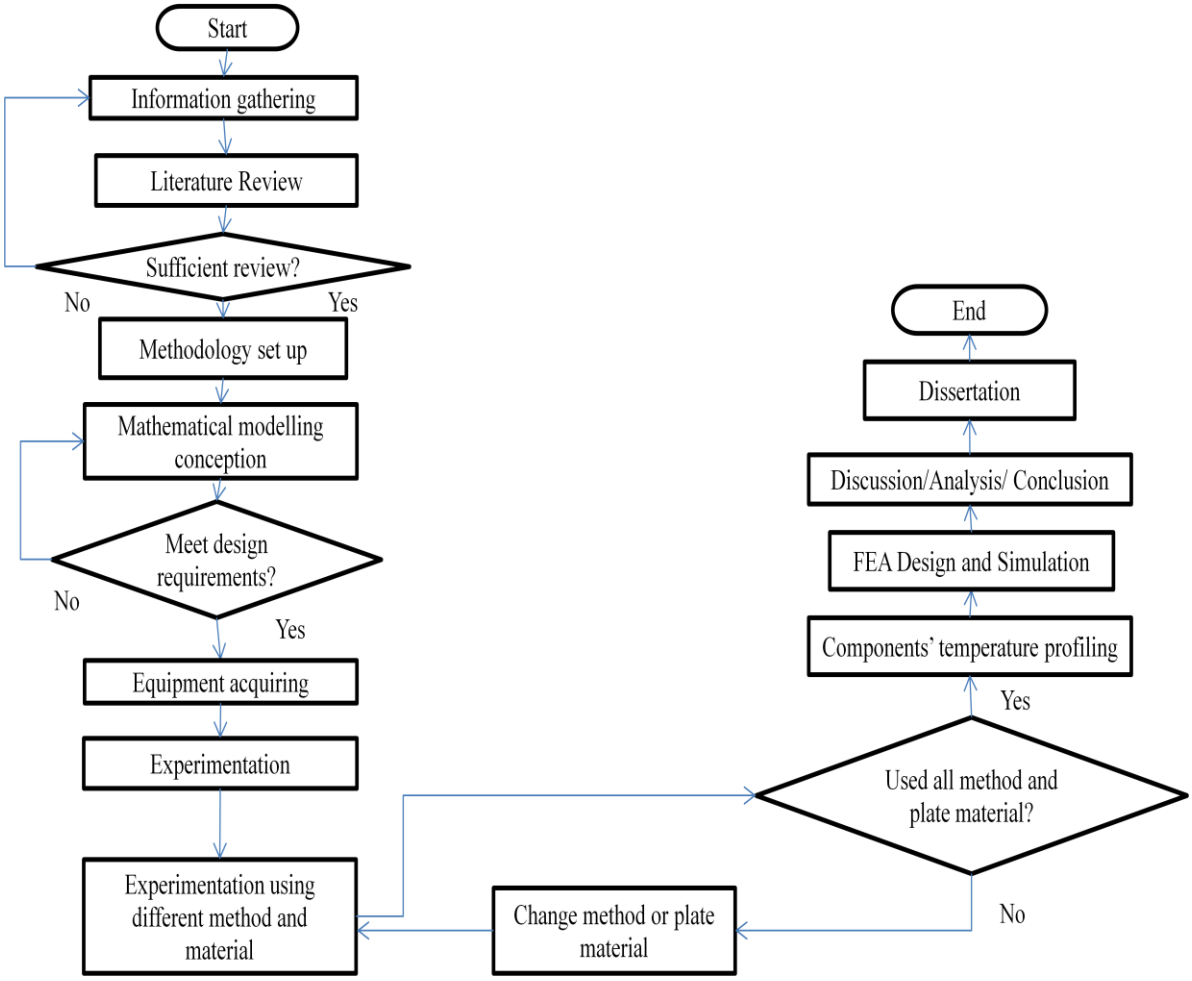

Figure 28: Methodology Flowchart

B) Gantt Chart

		FYP1 (Week)																FYP2 (Week)													
No	Tasks	1	2	3	4	5	6	7	8	9	10	11	12	13	14	15	16	1	2	3	4	5	6	7	8	9	10	11	12	13	14
1	Title selection																														
2	Title awarded																														
3	Information gathering																														
4	Project extended proposal																														
5	Proposal Defense																														
6	Draft Report																														
7	Interim Report																														
8	Mathematial Modelling Conception																														
9	Equipments Acquiring																														
10	Experimentation																														
11	Results Tabulation																														
12	Temperature Profiling																														
13	FEA Design and Simulation																														
14	Discussion and Conclusion																														
15	Poster Presentation																														
16	Final Report																														
17	Viva Presentation																														

Figure 29: Gantt Chart